CHAPTER IV
INVESTIGATION ON THE ROLES OF ACTIVATED CARBON SIZES ON METHANE HYDRATE FORMATION AND DISSOCIATION

4.1 Abstract

The presence of porous media such as activated carbon has been known to enhance the hydrate formation rate and the amount of gas consumption for methane storage applications. However, information on the effects of porous media particle size on the formation and dissociation kinetics is very limited or not available. Activated carbons with different particle sizes, 250-420 μm, 420-841 μm, and 841-1680 μm, were used in order to investigate their effects on the methane hydrate formation and dissociation. The methane hydrate formation experiments were conducted at 8 MPa and 4 °C in a quiescent fixed bed crystallizer. The result showed that the experiment conducted with the 841-1680 μm activated carbon showed the highest average water conversion to hydrate, 96.5 %, due to its large interstitial pore space between the activated carbon particles, which were observed by the two-step methane consumption. In contrast, the highest average percentage of methane recovery, 98.1 %, was achieved in the methane hydrate dissociation experiment conducted with the 250-420 μm activated carbon.

Keywords: Methane hydrate; Gas Hydrates; Hydrate formation; Hydrate dissociation; Activated carbon; Particle size

4.2 Introduction

In recent years, natural gas hydrates have gained much attention not only as a new source of natural gas but also as a means for novel applications like carbon dioxide capture, hydrogen storage and natural gas storage and transportation (Ding *et al.*, 2013; Englezos and Lee, 2005; Fan *et al.*, 2014; Kang and Lee, 2000; Kim *et al.*, 2011; Li *et al.*, 2010; Linga *et al.*, 2007; Mandal and Laik, 2008; Sloan, 2003; Veluswamy *et al.*, 2014). Natural gas hydrates, mainly methane, contain highly

concentrated methane gas. For example, 1 m^3 of methane hydrate contained 170 m^3 of methane gas at STP (Englezos and Lee, 2005). Although the natural gas hydrate reserve estimation is still debatable, it is widely believed that the amount of carbon in natural gas hydrates is more than twice the carbon content present in all the fossil fules combined (Kauda and Sandler 2005; Milkov, 2004; Sloan and Koh 2008). Once the hydrate is formed, mass transfer resistence of gas transport to liquid and eventually to hydrates results in the low water conversion to hydrate due to the formation of crystals at the interface (Erik *et al.*, 2001; Jiang *et al.*, 2008; Linga *et al.*, 2012; Fandiño and Ruffine 2014). Therefore, it is needed to have some methods to enhance the methane hydrate growth and the density of methane hydrate.

There are many methods to increase the hydrate formation rate and the diffusion rate between gas and water either by employing innovative reactor designs or by using promoters (thermodynamic or kinetic) (Babu *et al.*, 2013a; Florusse *et al.*, 2004; Linga *et al.*, 2010; Lv *et al.*, 2012). Florusse *et al.* (2004) added tetrahydrofuran (THF) to form hydrogen hydrate at low pressure by reducing the formation pressure from 300 MPa at 27 °C to 5 MPa ant 6.6 °C. A surfactant such as sodium dodecyl sulfate (SDS) was used by Ganji *et al.* (2007) to decrease the surface tension of water to increase the diffusion rate of gas into water. They reported that the methane hydrate formation rate and storage capacity were increased effectively, but the stability of the hydrate decreased. The effects of SDS on ethane hydrate were also studied by Mandal and Laik (2008). They demonstrated that the presence of SDS increased the gas consumption and affected the hydrate formation. Jiang *et al.* (2008) investigated the effect of mixed SDS-THF solution on the methane hydrate formation. They revealed that a small amount of SDS or THF can help to form hydrate very fast. Moreover, the rate of hydrate formation in the mixed SDS-THF solution was higher than in the one with and without SDS. Many papers reported the methane hydrate formation and dissociation with the presence of porous materials. Linga *et al.* (2009a) studied the methane hydrate formation in silica sand-water matrix at 8 MPa and 4 °C. The results showed the hydrate nucleation at multiple locations in the reactor, and more than 70 % of water can be converted to the hydrate. In the same year, Linga *et al.* (2009b) demonstrated the methane recovery from the hydrate formation in the presence of silica sand. The rate of methane

released depended on the bed size of silica sand, and there were two stages of hydrate dissociation. Recent works have shown that the methane hydrate formation rate and induction time was increased in the presence of multi-walled carbon nanotubes (MWCNTs) by changing the thermodynamic phase equilibrium of methane hydrate formation (Lim *et al.*, 2014; Park and Kim, 2010; Pasieka *et al.*, 2013). Chari *et al.* (2013) investigated the methane hydrate formation and dissociation in nano silica suspension. The results showed that the rate of methane hydrate formation in the presence of silica was increased compared to the system without the silica. Moreover, they revealed that the methane hydrate formation in silica was attributed to the dispersed water phase due to the silica large surface area. Babu *et al.* (2013b) studied the morphology of methane hydrate formation on silica sand and activate carbon. They reported that the hydrate crystals were formed in the interstitial pore space between the porous particles. Yan *et al.* (2005) studied the methane hydrate formation in wet activated carbon. They described that the storage capacity increased with the increase of the mass ratio of water to carbon. However, when the bulk water was higher than the carbon bed, the storage capacity was decreased. Liang *et al.* (2005) reported that methane hydrate dissociated faster with the presence of activated carbon than that of pure water. Moreover, they found the self-preservation effect in the experiment conducted at the temperature lower than the ice point. Recently, Siangsai *et al.* (2014) demonstrated that the activated carbon treated by sulfuric acid was more effective than that treated by potassium hydroxide in the methane hydrate formation.

Up till now, to our knowledge, there is no report on how particle size of porous media like activated carbon affects the methane hydrate formation. The particle size unavoidably plays an important role on the hydrate formation and dissociation. Therefore, this work reported the effects of activated carbon particle size on the methane hydrate formation and dissociation.

4.3 Experimental

4.3.1 Materials and Apparatus

Activated carbon, produced from coconut shell, was supported by Carbokarn Co., Ltd. Thailand. To investigate the effects of activated carbon particle size, the carbon was milled and sieved to 250-420 μm, 420-841 μm, and 841-1680 μm. The nitrogen adsorption analysis was carried out to measure the surface area, pore volume, and pore diameter of activated carbon by using an Autosorb-1MP gas sorption system (Quantachrome Corporation). The physical properties of activated carbon are shown in Table 4.1. It indicates that the properties of activated carbon are almost the same after milling, except the particle size that is noticeably different. Ultra high purity methane (99.999%, Labgaz Co., Ltd.) was used for the hydrate formation and dissociation experiment.

Figure 4.1a shows the schematic of gas hydrate apparatus, which consisted of a high-pressure stainless steel crystallizer (CR) and supply gas or a reservoir (R). The crystallizer and reservoir were immersed in a cooling bath, the temperature of which was controlled and adjusted by an external controllable circulator. Two pressure transmitters were used to measure the pressure. The temperature in the crystallizer was measured by four k-type thermocouples, located at different positions: T1 at the top of the bed, T2 at the middle of the bed, T3 at the bottom of the bed, and T4 at the bottom of the crystallizer, as seen in Figure 4.1b. A data logger (AI210 Model, Wisco Industrial instruments, Thailand) was connected to a computer to record the data during the experiment. All experiments were carried out in the quiescent condition with a fixed amount gas and water in the closed system.

4.3.2 Hydrate Formation Experiment

Approximately, 13 g of an activated carbon samples were placed in the crystallizer. The volume of water, required to fill the interstitial pore space of activated carbon bed (100 % water saturation), was at 1 cm^3 H_2O/1 g of carbon. The crystallizer was pressurized to 0.5 MPa and depressurized to atmospheric pressure twice to eliminate the presence of air bubble in the system. The temperature was set

to 4 °C and maintained by a controllable chiller. The crystallizer was pressurized to 6 MPa or 8 MPa. It took about 10 min for the temperature at different locations to reach the experimental temperature. The pressure and temperature profiles during this step for the typical methane hydrate formation experiment can be seen in Figure 4.2. After the pressure and temperature of the system reached the experimental condition, the data was then recorded every 10 s. During the hydrate formation, the pressure in the crystallizer was decreased due to the gas consumption. The experiments continued until there was no further pressure drop at least 1 h. The pressure and temperature data were used to calculate the methane consumption (mole of methane consumed). Hence, the moles of gas consumed for hydrate formation at time t is given by equation 4.1.

$$\Delta n_{H,\downarrow} = n_{H,0} - n_{H,t} = \left(\frac{PV}{zRT}\right)_{G,0} - \left(\frac{PV}{zRT}\right)_{G,t} \tag{4.1}$$

Here, $\Delta n_{H,\downarrow}$ is the number of moles of gas consumed for hydrate formation at the end of experiment. $n_{H,0}$ is the number of moles of hydrates at time zero. $n_{H,t}$ is the number of moles of the hydrates at time t. Subscripts of $G,0$ and G,t represent the gas phase at time zero and time t, respectively. P and T are the pressure and temperature in the syste. V is the volume of gas phase in the crystallizer. R is the universal gas constant. z is the compressibility factor calculated by Pitzer's correlation (Babu *et al.*, 2013b; Veluswamy and Linga, 2013).

4.3.3 Hydrate Dissociation Experiment

After completion of methane hydrate formation, the hydrate was dissociated by thermal stimulation. The pressure in the crystallizer was reduced carefully to the desired pressure at 6 MPa and 4.5 MPa by releasing the free gas in the system. Then, the temperature was increased from the formation temperature (4 °C) at the same heating rate for all experiments to 25 °C (temperature driving force (ΔT) of 21 °C). This point was marked as time zero for the dissociation experiment. The hydrate dissociates when the temperature in the crystallizer crosses the equilibrium phase boundary, corresponding to the desired experimental pressure. The

moles of methane released from the hydrate at any time during the hydrate dissociation can be calculated by equations 4.1 by replacing $\Delta n_{H,\downarrow}$ with $\Delta n_{H,\uparrow}$, which represents the number of moles of gas released from the hydrate. The methane recovery is calculated by equation 4.2 as a function of time for any dissociation experiment based on its information of formation experiment (Haligva *et al.*, 2010; Linga *et al.*, 2009b).

$$\% \text{ methane recovery} = \frac{(\Delta n_{H,\uparrow})}{(\Delta n_{H,\downarrow})} \tag{4.2}$$

4.4 Results and Discussion

4.4.1 Methane Hydrate Formation

The summary of methane hydrate formation experimental conditions is shown in Table 4.2. The experiments were carried out with three activated carbon sizes, including 250-420 μm, 420-841μm, and 841-1680 μm, and two experimental pressures of 6 MPa and 8 MPa. As seen from the table, for the experiments conducted at 8 MPa, the hydrate forms faster than at 6 MPa. Similar to the report by Linga *et al.* (2009a), the stochastic nature of hydrate nucleation can be observed in the table. In addition, the same phenomena can be seen with the different activated carbon sizes. Comparison among the different activated carbon sizes, it can be noted that the amount of methane hydrate consumption is influenced by the particle size at any given experimental condition. In addition, the final water conversion to hydrate is in the range of 71.5-98.7 % for all hydrate formation experiments.

4.4.1.1 Effect of Experimental Pressure

Figures 4.3a and 4.3b show the typical methane consumption and temperature profiles conducted with the activated carbon size of 841-1680 μm at 4 °C. As seen in Figure 4.3a, in the experiment conducted at 8 MPa (Experiment 13, Table 4.2), the methane hydrate forms immediately after introducing methane gas into the system. The hydrate formation can be observed by the heat released, seen in the temperature profiles in the figure. During the hydrate formation, methane uptake rapidly increases corresponding to the growth of the hydrate crystals in the space

between activated carbon particles, where the water is located. In addition, there is a subsequent hydrate nucleation during the experiment, which is evidenced by the temperature spikes. The results indicate that the methane hydrate can form randomly in the crystallizer. For the experiment 0 in Table 4.2 conducted with pure water, there is no hydrate formation until 48 h. This result can be explained that the hydrate formation might proceed systematically due to the layer-like film formation at the interface between water and gas and prevent the gas to consume for growing the hydrate crystals (Erik *et al.*, 2001; Fandiño and Ruffine, 2014; Linga *et al.*, 2012). This could be the reason that the hydrate formation in this sytem was not observed, while the presence of activated carbon increases the interfacial area between gas and water and allows the gas pass through the carbon bed. With the activated carbon, it is clear that the hydrate formation takes place in two steps, which is previously explained by Jin *et al.* (2012). First, the water that occupies between the porous particles, including the interconnectivity space and the interstitial space, is converted to hydrates, and a hydrate thin-film is formed (Jin *et al.*, 2012). When the hydrate is formed, the pore space becomes smaller leading to the increase in the capillary force in the narrow pore, which could inhibit the hydrate formation and lower the rate of hydrate growth (Clarke *et al.*, 1999; Anderson *et al.*, 2003; Jin *et al.*, 2012; Shicai *et al.*, 2014). However, Jin *et al.* (2012) also reported that the hydrate film formed in the pore space between porous particles could be cracked, resulting in the water from the cracks entering to the hydrate phase, where the second hydrate growth step is observed (Jin *et al.*, 2012). The results is further supported by Linga *et al.* (2009a), it was reported that the methane hydrate can be formed in the interstitial space between porous particles (Figure 4.4). This is why the methane uptake is increased again before reaching the plateau. The subsequent hydrate nucleation is also observed in the experiments conducted at 8 MPa with the 250-420 μm and 420-841 μm activated carbon. Figure 4.3b shows the typical methane consumption and temperature profiles of experiment conducted at 6 MPa with the activated carbon size of 250-420 μm (Experiment 16, Table 4.2). After introducing methane gas into the system, the gas diffuses into water before forming the hydrate, which can be seen at the beginning of methane consumption curve. After that, the hydrate starts to form by rapidly consuming methane gas. The temperature spikes correspond to the hydrate

nucleation in the crystallizer. Methane gas is continually consumed to grow the hydrate crystal until it reaches the equilibrium as observed in the experiment conducted at 8 MPa. The subsequent hydrate nucleation is also observed at 6 MPa, but it takes a longer time than at 8 MPa. Moreover, the amount of methane consumption at 6 MPa is lower than that at 8 MPa due to the pressure driving force.

To further clarify the effect of experimental pressure on the hydrate growth, Figure 4.5 presents the hydrate growth profiles during the methane hydrate formation conducted with the activated carbon size of 841-1680 μm at 4 °C. It can be deduced from the figure that the methane hydrate formation rate depends on the experimental pressure. In other words, the kinetics of methane hydrate formation is slow when the experimental pressure is decreased.

4.4.1.2 Effect of Particle Size

Figure 4.6 shows the comparison of the average hydrate growth during the methane hydrate formation with different particle sizes of activated carbon at 6 MPa and 4 °C. As seen form the figure, the experiments conducted with the small activated carbon particle size, 250-420 μm and 420-841 μm, show almost the same result of hydrate growth with no significantly different. On the contrary, the experiment conducted with the activated carbon size of 841-1680 μm shows a much lower hydrate growth rate. It can be deduced that the small particle size enhances the methane hydrate formation due to the high interconnectivity space between the particle packed in the crystallizer, as shown in Figure 4.4, which increases the contact area between methane gas and water. Therefore, the limitation of interconnected space in the larger size of activated carbon results in a slower methane hydrate formation rate than that of the small one (Babu *et al.*, 2013b).

Conversely, the average water conversions to hydrate at the end of experiment conducted at 6 MPa are 82.9 %, 80.4 %, and 75.5 % for the hydrate formation in the presence of activated carbon of 841-1680μm, 420-841 μm, and 250-420 μm, respectively. The results from the experiments conducted at 8 MPa show the same trend of the average water conversion to hydrate as those conducted at 6 MPa (Table 4.2). It can be concluded that the large particle size of activated carbon has a large interstitial space between the activated carbon particles, where the

subsequent hydrate can be formed, resulting in the high water conversion to hydrate. Consequently, it can be deduced from the methane hydrate formation experiments that the hydrate forms faster in the system with the small particle size than the one with the large particle size, but the highest amount of methane consumption is in the large particle size.

4.4.2 Methane Hydrate Dissociation

Table 4.3 summarizes the methane hydrate dissociation experimental conditions at 6 MPa and 4.5 MPa and temperature driving force (ΔT) of 21 °C. The experiment number in the table corresponds to the methane hydrate formation experimental conditions in Table 4.2. As seen from the table, the average rate of methane dissociated from the hydrate at 6 MPa is higher than that at 4.5 MPa with the same activated carbon size, but its methane recovery is somewhat lower. Moreover, the dissociation temperature of the experiment conducted at 6 MPa is higher than that at 4.5 MPa, corresponding to the methane hydrate phase equilibrium. In other words, methane hydrate dissociates at a higher temperature when the experimental pressure is increased. Furthermore, the final methane recovery is in the range of 79.2-99.1 % for all methane hydrate dissociation experiments.

Figure 4.7 shows the typical methane hydrate dissociation conducted with the 250-421 μm activated carbon at 6 MPa and temperature driving force (ΔT) of 21 °C. As seen in the figure, methane starts to release around 7.5 °C, which can be observed by the change in the temperature profiles of the thermocouples in the crystallizer due to the balance of heat transfer between the external heater and hydrate dissociation, which is an endothermic process. This temperature was marked as the dissociation temperature (T_d) at 6 MPa. The mole of methane gas obviously increases until it reaches the plateau. The temperature profiles, which were detected by the four thermocouples in the crystallizer, are different. Moreover, the temperatures from the four thermocouples indicate the hydrate dissociation regions. In other words, after the temperature crosses the equilibrium point or higher than the dissociation temperature, the temperature of thermocouples T1, T2, and T3 begins to increase simultaneously followed by T4. This observation indicates that the hydrate dissociation takes place in all regions once the temperature reaches the dissociation

temperature, but each region could take different times to complete the methane hydrate dissociation.

This observation can also be found in the experiments conducted at 4.5 MPa and with the activated carbon sizes of 250-420 μm, 420-841 μm, and 841-1680 μm. The completion of methane dissociation at each region can be clearly seen in Figure 4.8. This indicates that methane hydrate around thermocouple T2 region completes the hydrate dissociation followed by T4, T3, and T1, respectively. This result is different from the experiment conducted at 6 MPa (Figure 4.7). The different sequence of the methane hydrate dissociation regions depends on the formation of methane hydrate, which forms randomly in the activated carbon media, and the size of hydrates is also different at a given experimental condition. Therefore, the sequence of methane hydrate dissociation can be caused by the stochastic nature of the hydrate formation in the porous media.

4.4.2.1 Effect of Experimental Pressure

The comparison of the amount of methane released during the methane hydrate dissociation conducted with the activated carbon size of 420-841 μm is shown in Figure 4.9. It can be clearly seen in the figure that the amount of methane released from the system with the activated carbon size of 420-841 μm at 6 MPa is higher than that at 4.5 MPa. Moreover, the rate of methane released from the experiment conducted at 6 MPa is also higher than that at 4.5 MPa. This result can also be observed in the all experimental systems regardless of the size of activated carbon, as shown in Table 4.3.

4.4.2.2 Effect of Particle Size

Figure 4.10 shows the comparison of the rate of methane release and methane recovery from the hydrate dissociation experiment carried out at 6 MPa and ΔT=21 °C. As seen from the figure, the particle sizes of activated carbon have no significant effect on the rate of methane release. The experiment conducted with 841-1680 μm activated carbon shows the lower methane recovery than that the others, which is similar to the effect of particle size on the amount of methane consumption for hydrate formation experiment. The methane recovered from this work is between 79.2-99.1 %. High methane gas recovery, 94.7-99.1%, was reported by Linga *et al.* (2009b) with the presence of silica sand. They also reported that a

small amount of methane gas that was dissolved during the hydrate formation remained in water and was not recoverable.

From the experimental results, the effects of activated carbon particle size on the methane hydrate formation and dissociation are clearly demonstrated. In other words, the largest particle size of activated carbon shows the highest water conversion to hydrate, but the lowest methane recovery. The mechanism of methane hydrate formation in the presence of porous media was reported by Babu *et al.* (2013b) and Linga *et al.* (2009b). They revealed that, when the methane uptake reached the equilibrium, methane hydrate formed at the surface of porous media and grew up in the interstitial space between particles of porous media by the water from the cracks entering to the hydrate phase as previously discussed by Jin *et al.* (2012). A large interstitial space between the activated carbon particles is expected in the large activated carbon size. Once the methane hydrate is formed, it could form a large size of hydrate fitted in the interstitial space. When the temperature is increased, the methane hydrate crystals dissociate. In the case of the large size hydrate, the methane gas is released slower than a small one, as seen in Figure 4.10. Therefore, some methane molecules are still in the water after the methane hydrate dissociation. This probably explains why the methane recovery for all experiments is in the range of 79.2-99.1%.

4.5 Conclusions

The effects of activated carbon particle size on methane hydrate formation and dissociation were investigated. The results showed that all sizes of activated carbon enhanced the methane hydrate formation. The experiment conducted with the 250-420 μm activated carbon showed the fastest methane consumption to reach the equilibrium due to its increased contact area between methane gas and water via the interconnected space between the activated carbon particles. However, the experiment conducted with the 841-1680 μm activated carbon showed the highest methane consumption and water conversion to hydrate because of its large interstitial space between the activated carbon particles. Moreover, the average water conversion to hydrate for the methane hydrate formation with the presence of

activated carbon was in the range 75.5-96.5 %. In contrast, the experiment conducted with the activated carbon size of 250-420 μm exhibited the highest percentage of methane recovery for each experimental pressure of 6 MPa and 4.5 MPa in the methane hydrate dissociation experiment. The methane recovery was in the range 79.2-99.1 %.

4.6 Acknowledgements

This work was supported by The Royal Golden Jubilee Ph.D. Program (2.P.CU/51/J.1), Thailand Research Fund; The Petroleum and Petrochemical College (PPC), Chulalongkorn University, Thailand; National Metal and Materials Technology Center (MTEC)(MT-B-53-CER-09-269-G), Thailand; Center of Excellence on Petrochemical and Materials Technology (PETROMAT), Thailand; UOP, A Honeywell Company, USA.; National Univeristy of Singapore (R-279-000-420-750).

4.7 References

Anderson, R., Tohidi, B., and Webber, J.B.W. (2009) Gas hydrate growth and dissociation in narrow pore networks: capillary inhibition and hysteresis phenomena. Geological Society London Special Publications, 319(1), 145-159.

Babu, P., Kumar, R., and Linga, P. (2013a) Medium pressure hydrate based gas separation (HBGS) process for pre-combustion capture of carbon dioxide employing a novel fixed bed reactor. International Journal of Greenhouse Gas Control, 17(5), 206-214.

Babu, P., Yee, D., Linga, P., Palmer, A., Khoo, B.C., Tan, T.S., and Rangsunvigit, P. (2013b) Morphology of methane hydrate formation in porous media. Energy Fuels, 27, 3364-3372.

Chari, V.D., Sharma, D.V.S.G.K., Prasad, P.S.R., and Murthy, S.R. (2013) Methane hydrates formation and dissociation in nano silica suspension. Journal of Natural Gas Science and Engineering, 11, 7-11.

Clarke, M.A., Pooladi-Darvish, M., and Bishnoi, P.R. (1999) A Method to predict equilibrium conditions of gas hydrate formation in porous media. Industrial & Engineering Chemistry Research, 38, 2485-2490.

Ding, A., Yang, L., Fan, S., and Lou, X. (2013) Reversible methane storage in porous hydrogel supported clathrates. Chemical Engineering Science, 96, 124-130.

Englezos, P. and Lee, J.D. (2005) Gas hydrates—A cleaner source of energy and opportunity for innovative technologies. Korean Journal of Chemical Engineering, 22(5), 671-681.

Erik, M., Selim, M.S., and Sloan, Jr., E.D. (2001) Methane hydrate film growth kinetics. Fluid Phase Equilibria, 185, 65-75.

Fan, S., Yang, L., Wang, Y., Lang, X., Wen, Y., and Lou, X. (2014) Rapid and high capacity methane storage in clathrate hydrates using surfactant dry solution. Chemical Engineering Science, 106, 53-59.

Fandiño, O. and Ruffine, L. (2014) Methane hydrate nucleation and growth from the bulk phase: Further insights into their mechanisms. Fuel, 117, Part A, 442-449.

Florusse, L.J., Peters, C.J., Schoonman, J., Hester, H.C., Koh, C.A., Dec, S.F., Marsh, K.N., and Sloan, M.E. (2004) Stable low-pressure hydrogen clusters stored in a binary clathrate hydrate. Science, 306, 469-471.

Ganji, H., Manteghian, M., and Mofrad, H.R. (2007) Effect of mixed compounds on methane hydrate formation and dissociation rates and storage capacity. Fuel Processing Technology, 88, 891-895.

Haligva, C., Linga, P., Ripmeester, J.A., and Englezos, P. (2010) Recovery of methane from a variable-volume bed of silica sand/hydrate by depressurization. Energy Fuels, 24(5), 2947-2955.

Jiang, G., Tu, Y., Ning, F., Zhang, L., Dou, B., and Wu, X. (2008, July 6-10) Effect of SDS and THF on formation of methane-containing hydrates in pure water. Paper presented at The 6th International Conference on Gas hydrates (ICGH 2008). Vancouver, Canada.

Jin, Y., Konno, Y., and Nagao, J. (2012) Growth of methane clathrate hydrates in porous media. Energy Fuels, 26, 2242-2247.

Kang, S.P. and Lee, H. (2000) Recovery of CO_2 from flue gas using gas hydrate: Thermodynamic verification through phase equilibrium measurements. Environmental Science & Technology, 34, 4397-4400.

Kim, N.J., Park, S.S., Kim, H.T., and Chun, W.A. (2011) Comparative study on enhanced formation of methane hydrate using CM-95 and CM-100 MWCNTs. International Communications in Heat and Mass Transfer, 38, 31-36.

Klauda, J.B. and Sandler, S.I. (2005) Global distribution of methane hydrate in ocean sediment. Energy Fuels, 19, 459-470.

Li, X.S., Xu, C.G., Chen, Z.Y., and Wu H. (2010) Tetra-n-butyl ammonium bromide semi-clathrate hydrate process for post-combustion capture of carbon cioxide in the presence of dodecyl trimethyl ammonium chloride. Energy, 35(9), 3902-3908.

Liang, M., Chen, G., Sun, C., Yan, L., Liu, J., and Ma, Q. (2005) Experimental and modeling study on decomposition kinetics of methane hydrates in different media. Journal of Physical Chemistry B, 109, 19034-19041.

Lim, S.H., Riffat, S.B., Park, S.S., Oh, S.J., Chun, W., and Kim, N. (2014) Enhancement of methane hydrate formation using a mixture of tetrahydrofuran and oxidized multi-wall carbon nanotubes. International Journal of Energy Research, 38, 374-379.

Linga, P., Daraboina, N., Ripmeester, J.A., and Englezos, P. (2012) Enhanced rate of gas hydrate formation in a fixed bed column filled with sand compared to a stirred vessel. Chemical Engineering Science, 68, 617-623.

Linga, P., Haligva, C., Nam, S.C., Ripmeester, J.A., and Englezos, P. (2009a) Gas hydrate formation in a variable volume bed of silica sand particles. Energy Fuels, 23, 5496-5507.

Linga, P., Haligva, C., Nam, S.C., Ripmeester, J.A., and Englezos, P. (2009b) Recovery of methane from hydrate formed in a variable volume bed of silica sand particles. Energy Fuels, 23, 5508-5516.

Linga, P., Kumar, R., and Englezos, P. (2007) The clathrate hydrate process for post and pre-combination capture of carbon dioxide. Journal of Hazardous Materials, 149(3), 625-629.

Linga, P., Kumar, R., Lee, J.D., Ripmeester, J.A., and Englezos, P. (2010) A new apparatus to enhance the rate of gas hydrate formation: Application to capture of carbon dioxide. International Journal of Greenhouse Gas Control, 4(4), 630-637.

Lv, Q.N., Li, X.S., Xu, C.G., and Chen, Z.Y. (2012) Experimental investigation of the formation of cyclopentane-methane hydrate in a novel and large-size bubble column reactor. International Journal of Energy Research, 51(17), 5967-5975.

Mandal, A. and Laik, S. (2008) Effect of the promoter on gas hydrate formation and dissociation. Energy Fuels, 22, 2527-2532.

Milkov, A.V. (2004) Global estimates of hydrate-bound gas in marine sediments: How much is really out there? Earth-Science Reviews, 66, 183-197.

Park, S.S. and Kim, N.J. (2010, February 26-28) Multi-walled carbon nanotubes effects for methane hydrate formation. Paper presented at The 2nd International Conference on Computer and Automation Engineering (ICCAE), Singapore.

Pasieka, J., Coulombe, S., and Servio, P. (2013) Investigating the effects of hydrophobic and hydrophilic multi-wall carbon nanotubes on methane hydrate growth kinetics. Chemical Engineering Science, 104, 998-1002.

Shicai, S., Changling, L., Yuguang, Y., and Yufeng, L. (2014) Pore capillary pressure and saturation of methane hydrate bearing sediments. Acta Oceanologica Sinica, 33, 30-36.

Siangsai, A., Rangsunvigit, P., Kitiyanan, B., and Kulprathipanja, S. (2014) Improved methane hydrate formation rate using treated activated carbon and tetrahydrofuran. Journal of Chemical Engineering of Japan, 47(4), 352-357.

Sloan, E.D. (2003) Fundamental principles and applications of natural gas hydrates. Nature, 426, 353-359.

Veluswamy, H.P., Kumar, R., and Linga, P. (2014) Hydrogen storage in clathrate hydrates: Current state of the art and future directions. Applied Energy, 122, 112-132.

Veluswamy, H.P. and Linga, P. (2013) Macroscopic kinetics of hydrate formation of mixed hydrates of hydrogen/tetrahydrofuran for hydrogen storage. International Journal of Hydrogen Energy, 38, 4587-4596.

Yan, L., Chen, G., Pang, W., and Liu, J. (2005) Experimental and modeling study on hydrate formation in wet activated carbon. Journal of Physical Chemistry B, 109, 6025-6030.

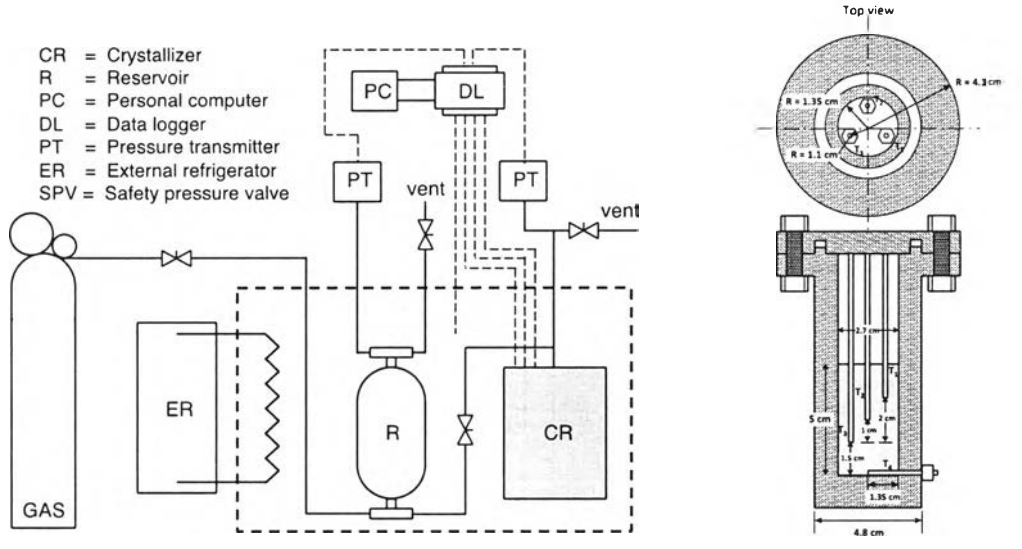

Figure 4.1 Schematic diagram of gas hydrate apparatus: a) schematic diagram, b) cross-section of a crystallizer

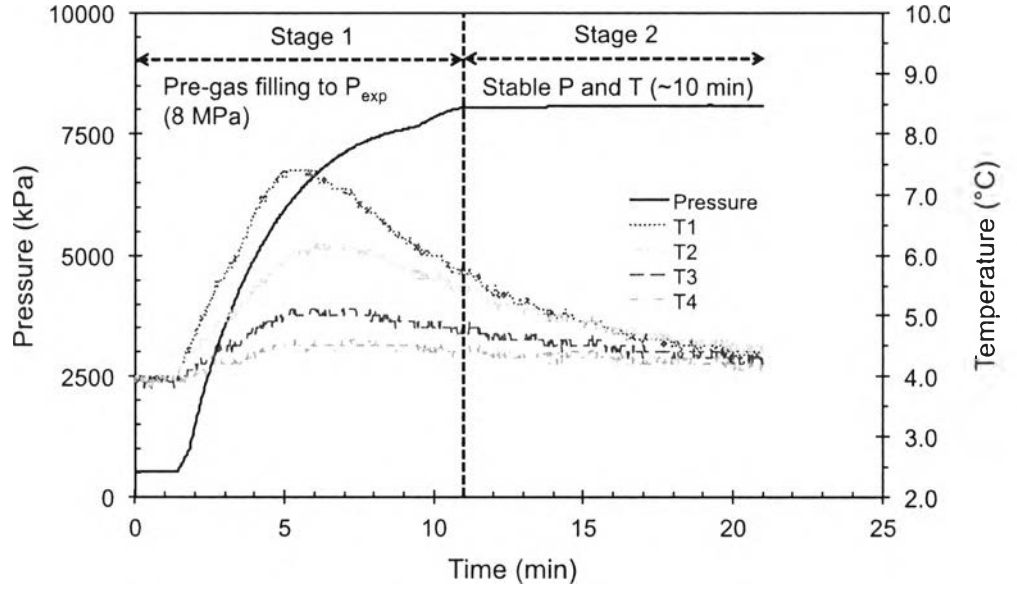

Figure 4.2 Typical pressure and temperature profiles of the experiment before the start of the experiment (Experiment 14). Stage 1 represents the pre-gas filling in the crystallzer, which was filled from the methane gas cylinder to reach P_{exp} (8 MPa). Stage 2 represents the time required to reach the constant of pressure and temperature.

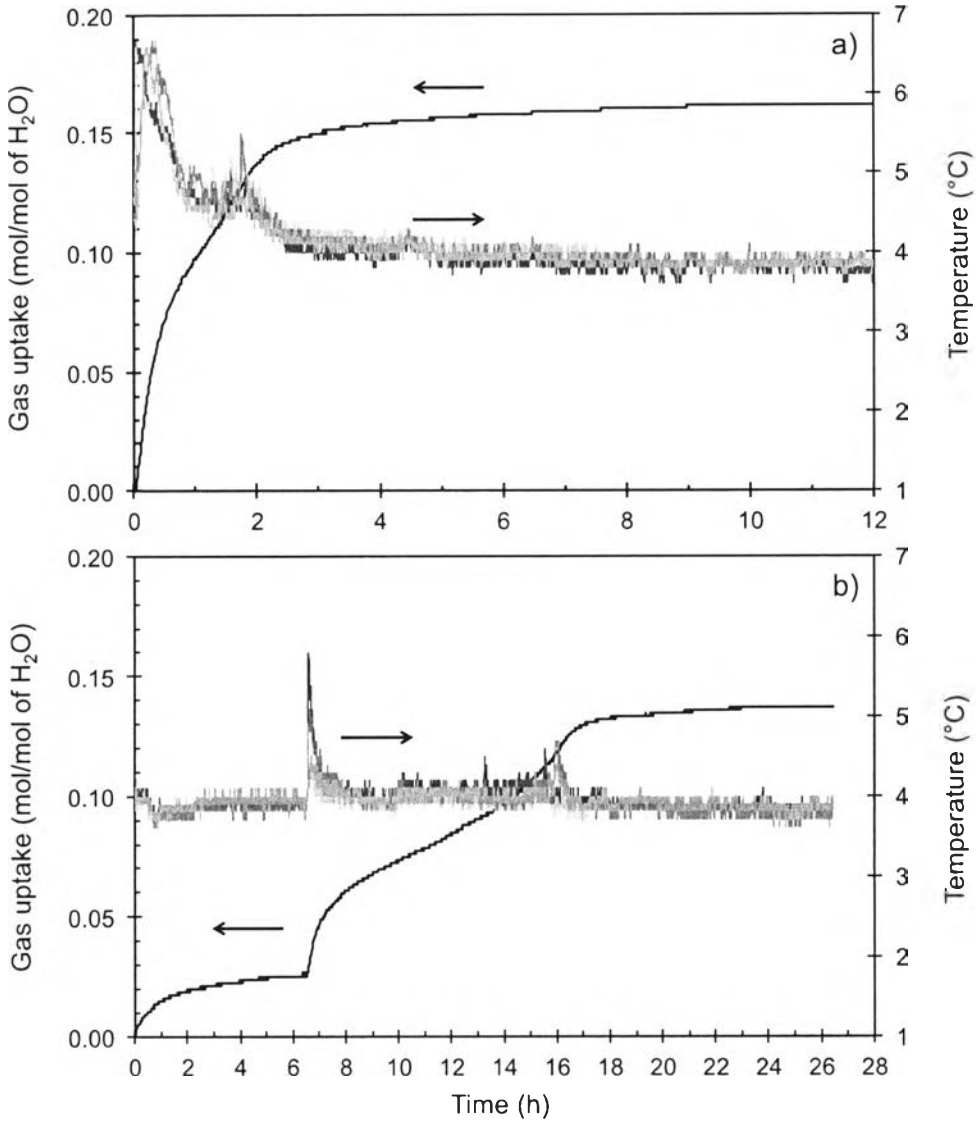

Figure 4.3 Typical methane consumption and temperature profiles during the methane hydrate formation experiments conducted with the activated carbon size of 841-1680 μm at 4 °C: a) 8 MPa (Experiment 13, Table 4.2), b) 6 MPa (Experiment 16, Table 4.2).

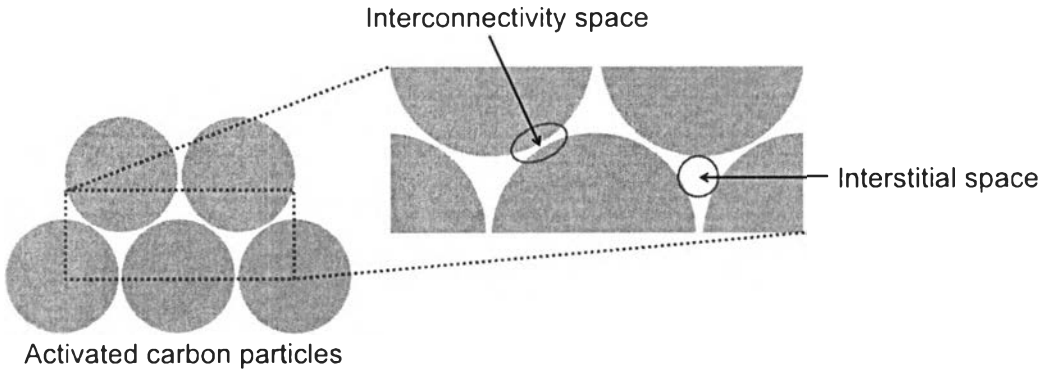

Figure 4.4 Illustration of the interstitial space and interconnectivity space.

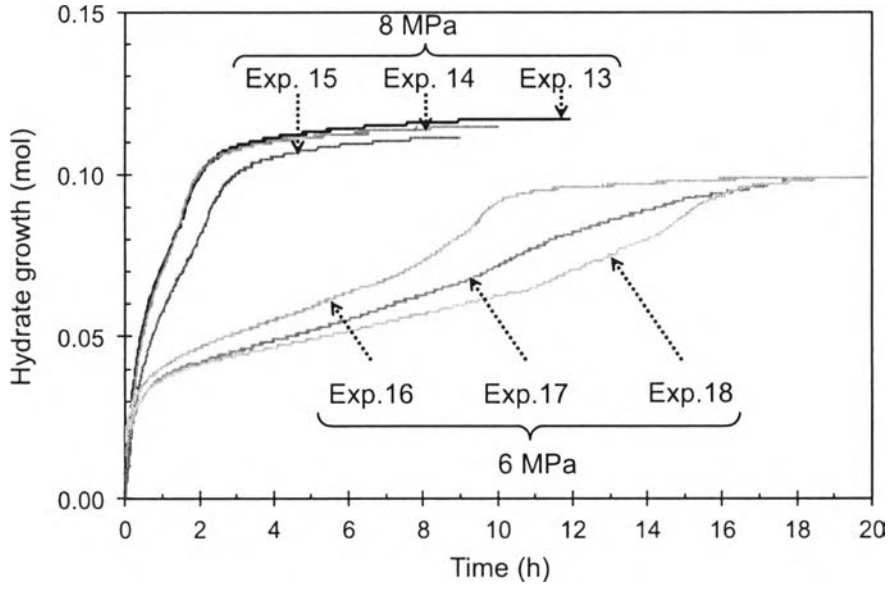

Figure 4.5 Hydrate growth profiles during the methane hydrate formation conducted with the activated carbon size of 841-1680 μm at 4 °C. (Time zero in the figures corresponds to the first point of hydrate growth.).

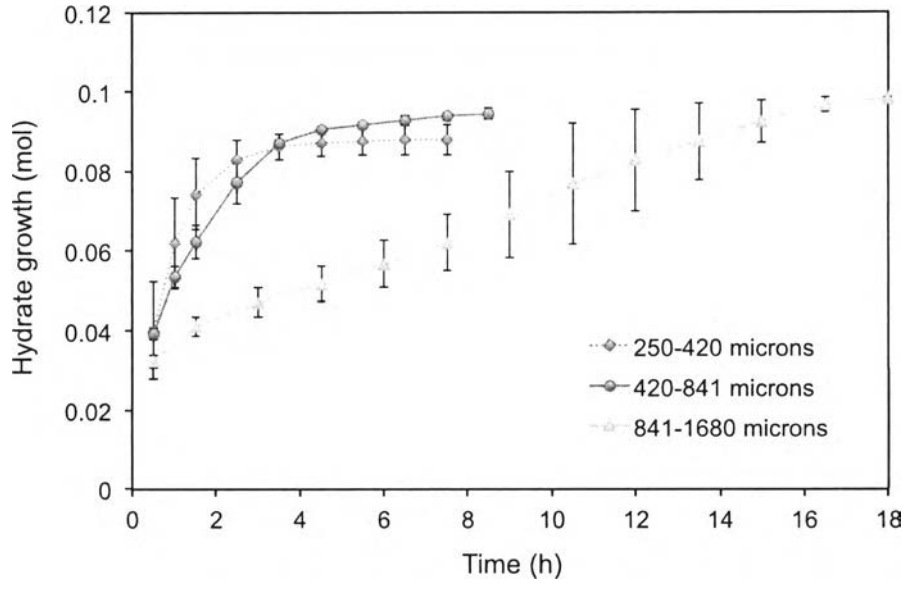

Figure 4.6 Comparison of the average hydrate growth during the methane hydrate formation at 6 MPa and 4 °C with the activated carbon particle sizes of 250-420 μm, 420-841 μm, and 841-1680 μm.

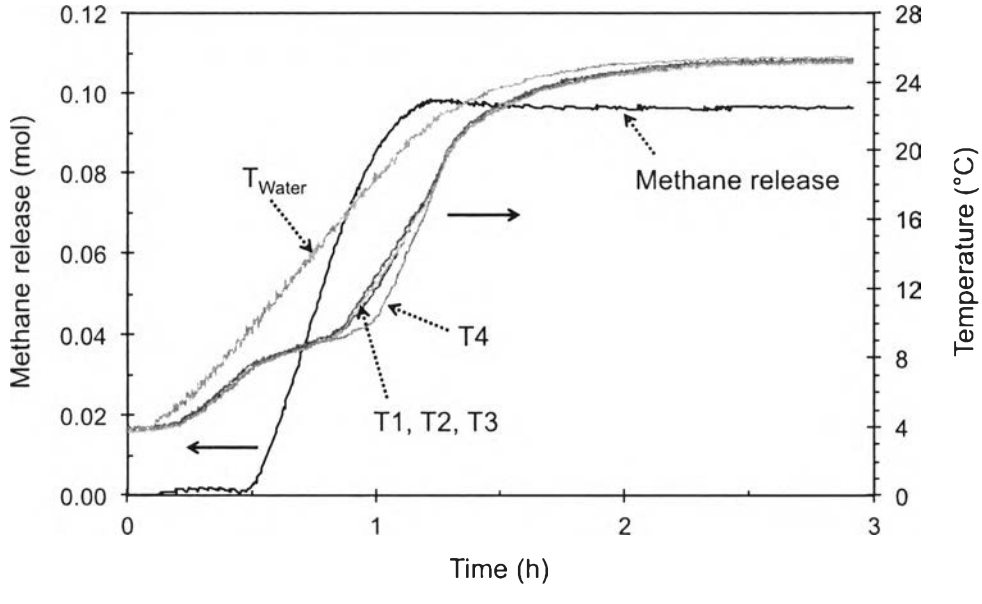

Figure 4.7 Typical methane dissociation and temperature profiles during the methane hydrate dissociation conducted with the activated carbon size of 250-420 μm at 6 MPa and ΔT=21 °C (Experiment 3, Table 4.3).

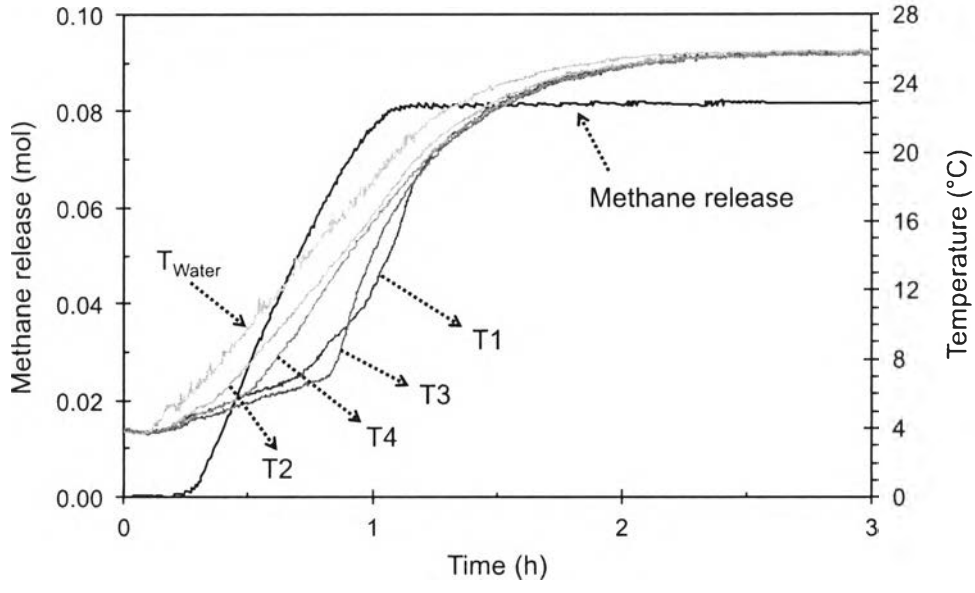

Figure 4.8 Typical methane dissociation and temperature profiles during the methane hydrate dissociation conducted with the activated carbon size of 841-1680 μm at 4.5 MPa and ΔT=21 °C (Experiment 16, Table 4.3).

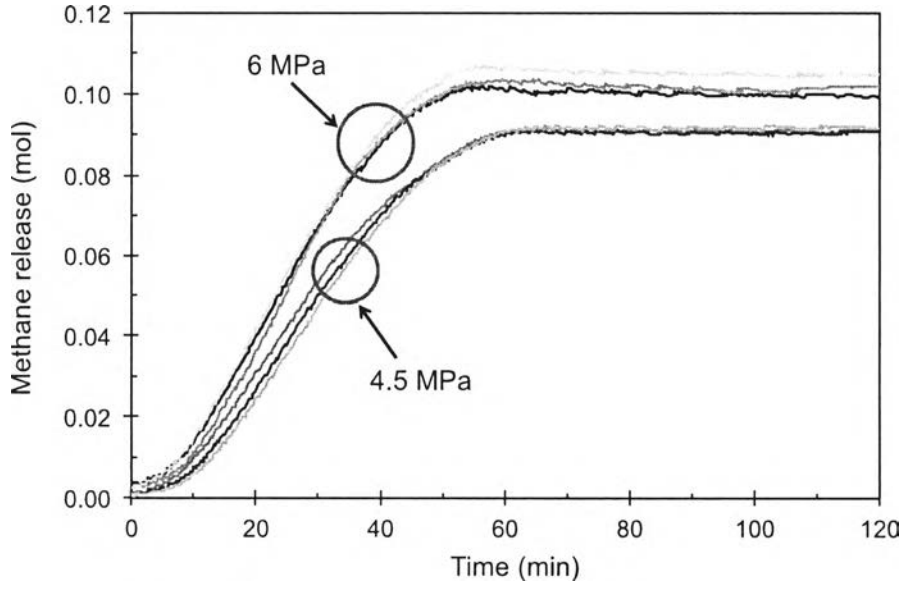

Figure 4.9 Comparison of methane dissociation conducted with the activated carbon size of 420-841 μm with different experimental pressure at ΔT=21 °C (Time zero in the figure corresponds to the first point of methane released.).

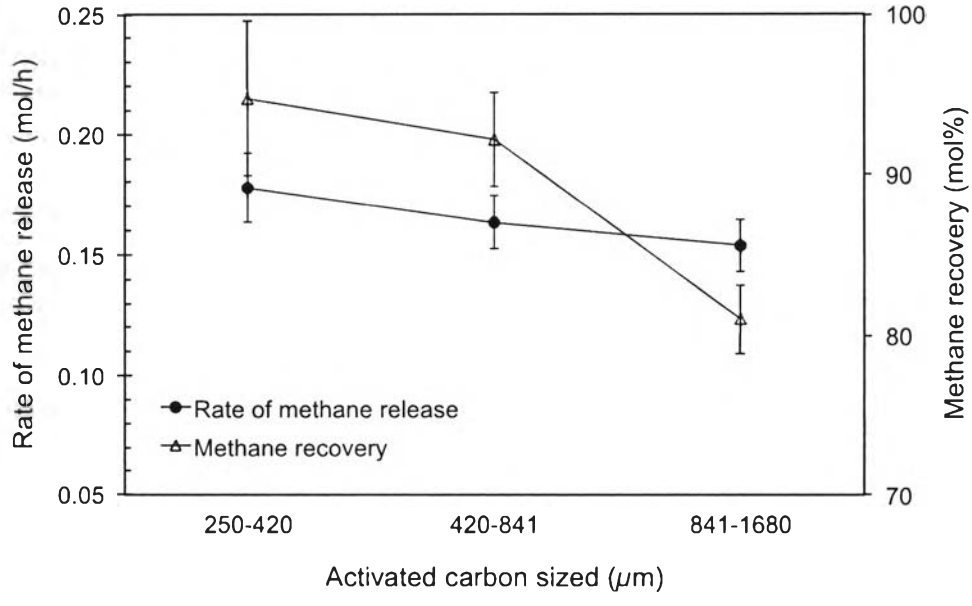

Figure 4.10 Comparison of the rate of methane release and methane recovery from the hydrate dissociation experiment carried out at 6 MPa and ΔT=21 °C.

Table 4.1 Physical properties of activated carbon

AC size (μm)	S_{BET} (m^2/g)	Total pore volume (cm^3/g)	Avg. pore diameter (nm)
250-420	864	0.51	2.18
420-841	877	0.48	2.19
841-1680	918	0.47	2.21

Table 4.2 Methane hydrate formation experimental conditions at 4 °C

Exp. No.	P_{exp} (MPa)	*Induction Time (min)	End of Experiment (h)	CH_4 Consumed (mol/mol of H_2O)	**Water Conversion to Hydrate (mol%)
			H_2O/CH_4		
0	8	NHF	-	-	-
			Activated carbon (250-420 μm)/H_2O/CH_4		
1	8	0.17	6.6	0.1507	91.9
2	8	0.17	1.3	0.1412	86.2
3	8	0.17	3.7	0.1371	83.6
			Average	**0.1430±0.0070**	**87.2±4.24**
4	6	540	21.1	0.1173	71.5
5	6	354	11.6	0.1278	78.0
6	6	1616	36.1	0.1261	76.9
			Average	**0.1237±0.0056**	**75.5±4.48**

NHF is no hydrate formation.

*Induction time is the first hydrate formation.

**Water conversion to hydrate (%) was calculated using the hydration number of 6.1.

Table 4.2 Methane hydrate formation experimental conditions at 4 °C (*Cont.*)

Exp. No.	P_{exp} (MPa)	*Induction Time (min)	End of Experiment (h)	CH_4 Consumed (mol/mol of H_2O)	**Water Conversion to Hydrate (mol%)
			Activated carbon (420-841 μm)/H_2O/CH_4		
7	8	2.33	8.6	0.1506	91.9
8	8	0.17	7.6	0.1574	96.0
9	8	2.00	7.8	0.1519	92.7
			Average	**0.1533±0.0036**	**93.5±2.17**
10	6	1349	32	0.1333	81.3
11	6	1652	35.4	0.1297	79.2
12	6	1240	32.3	0.1322	80.7
			Average	**0.1317±0.0018**	**80.4±1.08**
			Activated carbon (841-1680 μm)/H_2O/CH_4		
13	8	2.00	11.9	0.1618	98.7
14	8	0.33	10.1	0.1583	96.6
15	8	3.33	9.1	0.1543	94.1
			Average	**0.1581±0.0038**	**96.5±2.30**
16	6	394	26.5	0.1369	83.5
17	6	256	22.6	0.1356	82.7
18	6	873	33	0.1355	82.6
			Average	**0.1360±0.0008**	**82.9±0.49**

NHF is no hydrate formation.

*Induction time is the first hydrate formation.

**Water conversion to hydrate (%) was calculated using the hydration number of 6.1.

Table 4.3 Hydrate decomposition experimental conditions at *ΔT = 21 °C

Exp. No.	P_{exp} (MPa)	**T_d at P_{exp} (°C)	Rate of Methane Dissociation (mol/h)	Methane Recovery (mol%)
		Activated carbon (250-420 μm)/H_2O/CH_4		
1	6	6.4	0.1855	97.8
2	6	6.7	0.1613	89.2
3	6	6.9	0.1869	97.2
		Average	**0.1779±0.0144**	**94.7±4.80**
4	4.5	4.6	0.1350	96.2
5	4.5	4.6	0.1446	99.1
6	4.5	4.2	0.1362	98.9
		Average	**0.1386±0.0052**	**98.1±1.62**
		Activated carbon (420-841 μm)/H_2O/CH_4		
7	6	6.6	0.1513	92.4
8	6	6.5	0.1732	89.1
9	6	6.4	0.1660	95.0
		Average	**0.1635±0.0112**	**92.2±2.96**
10	4.5	4.5	0.1366	94.8
11	4.5	4.6	0.1355	96.3
12	4.5	4.6	0.1372	96.1
		Average	**0.1364±0.0009**	**95.7±0.81**

*ΔT is the temperature driving force ($\Delta T = T_{end} - T_{start}$).

**T_d is the dissociation temperature at which methane releases for the experimental pressure, P_{exp}.

Table 4.3 Hydrate decomposition experimental conditions at *ΔT = 21 °C (*Cont.*)

Exp. No.	P_{exp} (MPa)	**T_d at P_{exp} (°C)	Rate of Methane Dissociation (mol/h)	Methane Recovery (mol%)
		Activated carbon (841-1680 μm)/H_2O/CH_4		
13	6	6.9	0.1617	80.4
14	6	6.6	0.1414	79.2
15	6	6.9	0.1583	83.3
		Average	**0.1538±0.0109**	**81.0±2.11**
16	4.5	4.8	0.1179	82.6
17	4.5	4.7	0.1233	84.2
18	4.5	4.8	0.1243	84.2
		Average	**0.1218±0.0034**	**83.7±0.92**

*ΔT is the temperature driving force ($\Delta T = T_{end} - T_{start}$).

**T_d is the dissociation temperature at which methane releases for the experimental pressure, P_{exp}.